Journal of Materials Chemistry C

ROYAL SOCIETY OF CHEMISTRY

PAPER

View Article Online
View Journal | View Issue

Cite this: J. Mater. Chem. C, 2021, 9, 17371

Electrical transport properties of EuTe under high pressure†

Yuqiang Li, *[ab] Jingxia Liu, [ab] Peiguang Zhang,[c] Qiang Jing, [d] Xiaofeng Liu,[e] Jianxin Zhang,[a] Ningru Xiao,[b] Liyuan Yu[a] and Pingjuan Niu*[ab]

Received 28th June 2021,
Accepted 12th November 2021

DOI: 10.1039/d1tc02941j

rsc.li/materials-c

The pressure-induced electronic and optical properties of EuTe were investigated up to 35.6 GPa. Using first-principles calculations, it was found that EuTe undergoes a pressure-induced NaCl–CsCl structural transition above 13 GPa. The metallic character of EuTe is strengthened with an increase in pressure, according to the calculation results of band structure and electron density of states. EuTe is observed to undergo semiconductor-to-semimetal transition when the Fermi surface is crossed only by the spin-up band at 6 GPa, and the metallization transition is shown at 13 GPa. The structural phase transition of EuTe is reflected at approximately 13.8 GPa based on the discontinuous electrical parameters, and the abrupt decrease of resistivity is caused by a joint increase in the carrier concentration and mobility, while the abrupt decrease of Hall coefficient is attributed to the increase of carrier concentration. The metallization transition is also evidenced at 13.8 GPa by temperature-dependent resistivity. The discontinuous changes in the optical parameters at around 6.9 GPa and 13.8 GPa are caused by semiconductor-to-semimetal transition and structural phase transition, respectively. The transition pressure is reduced in the presence of light, occurring at approximately 12.7 GPa.

Introduction

Europium telluride (EuTe) is a semiconductor with a band gap of about 1.96 eV, and it has a simple NaCl structure (space group: $Fm\bar{3}m$, No. 225, $Z = 6$) and pure spin magnetism.[1] The magnetic properties of EuTe have been extensively investigated because of its strong localized moments, which make it a classical Heisenberg magnet.[2] It has been demonstrated that huge magnetic polarons are generated in EuTe by light.[3] EuTe has become an important functional material due to these interesting features, being particularly suitable for the study of magnetic semiconductors,[4–6] and it holds great potential for applications in spintronics and optics.[7–11] The properties of EuTe are largely influenced by the rare earth element Eu. Eu atoms have a unique electronic structure, with a 4f electron shell layer in a half-filled state, and there is a strong correlation effect bringing about many novel physical phenomena. The valence instability of Eu atoms also makes its compounds' resistivity and magnetization undergo abnormal changes under pressure. Compounds of other rare earth elements, such as Ni, Sm, Ce and La, also exhibit exceptional optical, electronic, magnetic and catalytic properties.[12–16] Therefore, EuTe, as a representative rare earth element compound, has always been the object of extensive attention from scientific researchers.

High pressure, as an effective means to change the physical properties of crystals,[17–19] makes the volume of matter smaller, shortens the distance between atoms, changes the crystal structure and the behavior of electrical transmission, and even leads to superconductivity;[20–22] high-pressure experiments are also very suitable for exploring the magnetic transition of matter.[23,24] Therefore, applying high pressure is an important way to discover functional materials with novel electrical and optoelectronic properties. By studying the high-pressure electronic structure and optical properties of EuTe, the development of both high-pressure science and the materials field will be driven by both experimental and theoretical approaches to study EuTe.

[a] Tianjin Key Laboratory of Optoelectronic Detection Technology and Systems, School of Electrical and Electronic Engineering, Tiangong University, Tianjin 300387, China. E-mail: liyuqiang@tiangong.edu.cn, niupingjuan@tiangong.edu.cn
[b] Engineering Research Center of High Power Solid State Lighting Application System of Ministry of Education, Tiangong University, Tianjin 300387, China
[c] State Key Laboratory of Applied Optics, Changchun Institute of Optics, Fine Mechanics and Physics (CIOMP), Chinese Academy of Sciences, Changchun 130033, China
[d] Laboratory of Functional Molecules and Materials, School of Physics and Optoelectronic Engineering, Shandong University of Technology, Zibo 255000, China
[e] Tianjin San'an Optoelectronics Co., LTD., Tianjin 300384, China

† Electronic supplementary information (ESI) available: (i) EuTe geometry optimization results, (ii) experimental parameters for the preparation of microcircuits, (iii) Energy band of EuTe (NaCl) at 12.5 GPa, (iv) density of states ender different pressure, and (v) density of states of NaCl and CsCl structures at 13 GPa. See DOI: 10.1039/d1tc02941j

Singh *et al.* used the first-principles local density approximation (LDA) algorithm to calculate EuTe and found that the structural phase transition from NaCl to CsCl structure (space group: $Pm\bar{3}m$, No. 221, Z = 8) occurred at 9.89 GPa, and the valence configuration did not change significantly.[25] The NaCl-to-CsCl transition of EuTe at 13 GPa was reported by Petit *et al.*[26] It is found that NaCl and CsCl structures coexist in the range of 13–17 GPa; the structure of CsCl is completely converted at 17.3 GPa, and there is no magnetic transformation in the high-pressure-phase CsCl structure, according to the neutron diffraction study of EuTe conducted by Goncharenko *et al.*[27] The compressibility of the monotellurides of Pr, Sm, Eu, Tm, and Yb and the monoselenide and sulfide of Sm has been investigated to 300 kbar using high-pressure X-ray diffraction techniques, which show that EuTe exhibits a phase transition from NaCl-type to CsCl-type structure at pressures of about 110 ± 10 kbar.[28] EuTe was found to undergo a pressure-induced transition from antiferromagnetic to ferromagnetic order at approximately 8 GPa pressure by uniform magnetization measurement of a very small sample in a diamond anvil cell by Ishizuka *et al.*[29]

The electrical transport structure of EuTe is directly related to the magnetic properties in many aspects, as observed by Shapira *et al.* Meanwhile, the abrupt changes in $d\rho/dK$ and $d\rho/dH$ imply a shift from oblique to paramagnetic, in studying the dependence of resistivity, the Hall coefficient, on temperature *versus* magnetic field.[30,31] Also, it was shown that the large negative magnetoresistance generated at low temperatures is mainly due to changes in mobility rather than the carrier concentration through Hall effect measurements on single-crystal EuTe.[32] In a magnetic field up to 28 T, the luminescence characteristics of the magnetopolaron in EuTe have been explored through theory and experiment. Studies demonstrated that as the energy of the pump photon increases above the band gap, the photogeneration efficiency of the polariton becomes less and less efficient. The luminescence properties of the magnetic polariton in EuTe were explored theoretically and experimentally when the magnetic field was up to 28 T.[33] The band-edge optical absorption of EuTe was studied in the framework of the 5d conduction band atomic model by Henriques *et al.* The results show that for the ferromagnetic arrangement, the absorption exhibits a huge dichroic bimodal peak with narrow lines. In the antiferromagnetic arrangement, the spectrum is blue shifted, becoming broader and weaker, and the dichroism is suppressed.[34]

Most of the studies have focused on the areas of high-pressure structural properties, magnetic properties, and electrical and optical properties at atmospheric pressure in the abovementioned content, but there are few reports on the modulation of the optical and electrical properties of EuTe by applying pressure. In this work, the electronic and optical properties of EuTe were theoretically and experimentally investigated. At 6 GPa, the transition from semiconductor to semimetal is evidenced by the spin-up energy band passing through the Fermi surface. Semimetal-to-metal transition was observed at 13.8 GPa based on the temperature-dependent resistivity, and the discontinuous change in the slope of the electrical parameters was related to the pressure-induced phase transition. An abrupt change in optical parameters was also caused by the semiconductor–semimetal–metal transition.

Theoretical basis

EuTe exhibits the sodium chloride (NaCl) structure under atmospheric conditions, which is face-centered cubic, with six atoms of opposite type, and the space group $Fm\bar{3}m$ at atmospheric pressure.[35] Eu^{2+} is bonded to six equivalent Te^{2-} atoms to form a mixture of edge- and corner-sharing octahedra, exhibiting the appearance of each ion surrounded by six others, and all with an Eu–Te bond length of 3.27 Å. The lattice parameters $a = b = c = 6.59$ Å, with Eu and Te atoms occupying the positions (0, 0, 0) and (0.5, 0.5, 0.5), according to the experimental values.[25] The space group of the CsCl structure is $Pm\bar{3}m$ for EuTe, with Eu and Te atoms occupying the positions (0.5, 0.5, 0.5) and (0, 0, 0).

All computational tasks were performed through the Cambridge Sequential Total Energy Package (CASTEP)[36] software package, which is based on the first-principles density generalized function theory. The electronic exchange–correlation potential is processed by the Perdew–Burke–Ernzerhof (PBE) function of generalized gradient approximation (GGA), and the structure optimization adopts the minimum calculation rule Broyden–Fletcher–Goldfarb–Shanno (BFGS) technology.[37] The energy cutoff is set to 480 eV; the Monkhorst–Pack *k*-point grid for EuTe is 6 × 6 × 6; and the self-consistent convergence accuracy is set to 2.0×10^{-6} eV per atom. The convergence parameters are 1.0×10^{-5} eV for energy, 0.03 eV Å^{-1} for maximum force, 0.05 GPa for maximum stress, and 0.001 Å for maximum displacement. The 4f orbital of the rare earth element Eu atom has 7 electrons, which indicates that the electrons should preferentially occupy different orbitals with the same spin direction to have the lowest crystal energy, according to Hundt's rule and Pauli exclusion principle. This generates a spin magnetic moment because the outermost electrons have the same spin direction, so the spin state should be considered to obtain more accurate results. Furthermore, it is worth considering correcting the Coulombic force between electrons by introducing a U value, $U_f = 5$ eV, allowing the GGA to accurately describe the electronic structure of strongly correlated electronic systems (see ESI,† Table S1).

Experimental

Integration of microcircuits

The high pressure required for the experiments was generated by a diamond anvil cell (DAC), and the anvil culet was 300 μm in diameter with a bevel angle of 10°. High-pressure *in situ* electrical experiments of EuTe are studied by microcircuits, which are integrated on the diamond anvil surface by photolithography.[38,39] First, a thin metal-molybdenum film is deposited on a clean diamond anvil, then a cross is etched in the center of the film to divide it into four electrode regions by using photolithography, and finally, the insulating varnish is

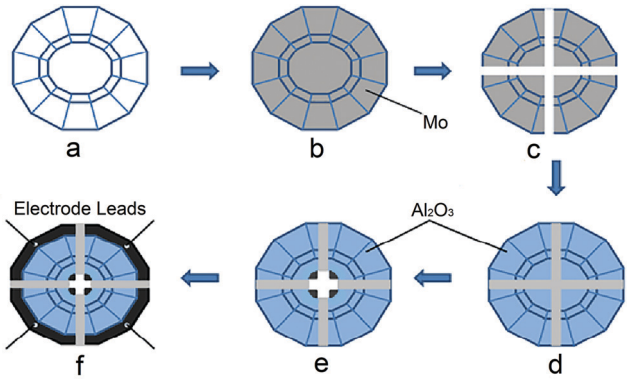

Fig. 1 Microcircuit integration process. (a) Clean diamond; (b) sputter a Mo thin film on the diamond anvil as electrode material; (c) perform photolithography on the Mo thin film and etch a cross to divide the electrode into four regions; (d) sputter the Al_2O_3 thin film as the insulating protective thin film of the electrode onto the metal molybdenum film; (e) photolithography of Al_2O_3 thin film, etching a detection window on the diamond anvil; (f) remove the Al_2O_3 thin film on the electrode leads, thus completing the production of integrated microcircuits.

removed from the enameled wire with a diameter of 100 μm, using conductive silver paste to connect it to the four metal molybdenum electrodes. It is necessary to use magnetron sputtering technology to deposit a thin film of Al_2O_3 on the molybdenum electrode to protect the molybdenum electrode and achieve the effect of insulation with the metal spacer under high pressure. The microcircuit integration process is shown in Fig. 1, and the experimental parameters (see ESI† Tables S2–S4) are given.

High-pressure experiments

High-pressure *in situ* electrical experiments were performed under non-hydrostatic conditions.[40] It is essential to make an insulating spacer to ensure the accuracy of the measurement results of high-pressure *in situ* electrical experiments and to prevent an electric short caused by contact between the sample and the inner wall of the metal spacer. The manufacturing process for the insulating gasket is basically the same as that reported in a previous article,[41] which consists of pre-pressing the T301 stainless steel sheet to 80 μm, then drilling a hole with a diameter of 150 μm in the center of the indentation. The diamond powder, glue, and polymethylmethacrylate (PMMA) are fully mixed and filled into the indentation area of the gasket, and a hole with a diameter of 80 μm is drilled in the center of the indentation using a laser, which is used as a sample chamber. A piece of ruby crystal used for pressure calibration is placed in the center of the sample chamber.[42,43] The resistivity and Hall effect of EuTe were measured by the van der Pauw method.[44] The current was measured using a Keithley 2400 source meter, and the voltage with a Keithley 2700 multimeter. The EM7 electromagnet produced by East Changing Company produces a uniform magnetic field, and the magnetic field was measured by a Lakeshore 420 Gauss meter.

Sample synthesis

The single crystal of EuTe was grown by self-flux method. Eu pieces and Te powder were mixed in a molar ratio of 1 : 1 and put into an alumina crucible, then sealed in an evacuated quartz tube under 2×10^{-4} Pa to avoid oxidization during the reaction. The quartz tube with alumina crucible was placed in a muffle furnace and heated to 650 °C over 5 h, then the sample was kept at 650 °C for 24 h, after which the muffle furnace was turned off to let the sample cool to room temperature. Next, the sample was re-ground and pressed into a tablet in the glove box. Then, the sealing procedure was repeated. After that, the quartz tube with alumina crucible was again heated to 650 °C over 5 h. After keeping the sample at 650 °C for 24 h, it was slowly cooled to 600 °C over 24 h, then the muffle furnace was turned off to let the sample cool to room temperature again.

Results and discussion

Structural phase transition

The most stable structure is the one that possesses the lowest Gibbs energy at a given temperature, which is known from thermodynamic theory. CASTEP software simulates the result of the ground state at zero temperature, so $G = U + pV = H$, where U is the intracellular energy; V is the cell volume; and p is the cell pressure. It is obvious that the phase transition order and phase transition pressure of the crystal can be determined when the enthalpies of the two phases are equal.[45,46] Fig. 2 shows the relationship between the enthalpy value of the two crystal structures and pressure. It can be clearly seen that the structural phase transition from the NaCl structure to the cesium chloride structure (CsCl) occurs at about 13 GPa, when the enthalpy of the two structures changes significantly, with the enthalpy of the CsCl structure being lower than the enthalpy of the NaCl structure.

The EuTe structure crystallizes in the cubic $Pm\bar{3}m$ space group. Eu^{2+} is bonded in a body-centered cubic geometry to eight equivalent Te^{2-} atoms, and all Eu–Te bond lengths are 3.50 Å. The phase transition sequence is consistent with that reported in the previous literature,[25] and the phase change

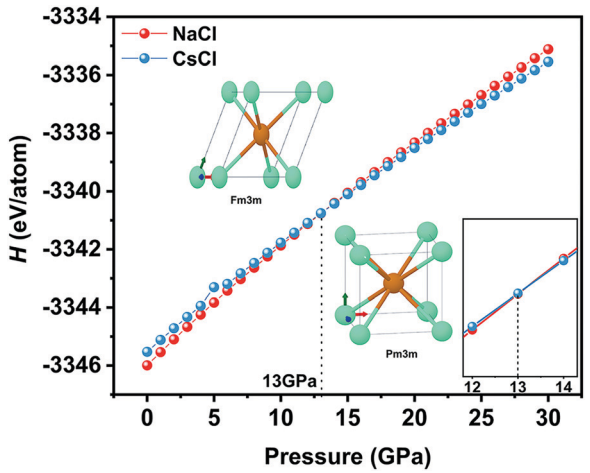

Fig. 2 Relationship between EuTe enthalpy and pressure, and the primitive cell structure diagrams of the two structures are given.

pressure point of 13 GPa differs from the 11 GPa reported in the literature,[47] but this difference is acceptable. CASTEP performing an approximate theoretical simulation calculation is the main reason for the error; a typical reason is that the calculation temperature is 0 K based on CASTEP default, while the experiment is done at room temperature. The pathway to prove the occurrence of phase transition is not only through the principle of enthalpy equivalence but also the collapse of the relative volume of EuTe and the sudden change in elastic properties, which likewise confirm the occurrence of phase transition, as reported by Gupta *et al.*[48]

First-principles calculations of the electronic and optical properties

Energy band theory is an approximation theory that describes the motion of electrons in a crystal in a periodic potential field; it can be used to analyze the conductivity of crystals and atomic interactions. Energy band diagrams of EuTe for different pressure values were obtained by applying pressure. Fig. 3(a and b) shows the energy bands of NaCl structure at 0 GPa and 13 GPa, respectively; it can be clearly seen from Fig. 3a that at 0 GPa, both the spin-up and spin-down Fermi surfaces of EuTe do not cross the energy band, forming a band gap of 0.738 eV, with EuTe behaving as an indirect band gap semiconductor due to the highest point of the valence band being at Γ point and the lowest point of the conduction band at the high-symmetry X point.

There is some difference between the theoretical and experimental band gap values at atmospheric pressure, which may be related to the usually underestimated value of band gap energy by density functional theory (DFT).[49] The research focuses on the relative change trend of the band gap of EuTe under pressure. Although the calculated absolute value of the band gap slightly deviates from the experimental value, it will not affect the later analysis of the band gap change law.

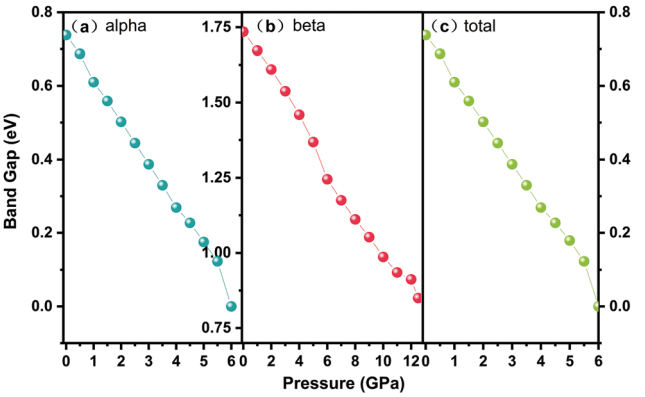

Fig. 4 The band gap of EuTe under high pressure. (a) Spin-up band gap value, (b) spin-down band gap value, (c) total band gap value.

The band gap variation of EuTe with NaCl structure under different pressures is shown in Fig. 4, which includes the (a) spin-up band gap value, (b) spin-down band gap value, and (c) total band gap value. It can be seen that EuTe has a semiconducting nature until 6 GPa (Fig. 4c) due to the existence of spin-up and spin-down band gap values before then (Fig. 4a and b). As the total band gap value decreases to 0 eV at 6 GPa with applied pressure, combined with Fig. 3b, it can be seen that the reduction of the band gap value to 0 eV at 6 GPa is caused by the spin-up energy band. At this time, the spin-up energy band broadens across the Fermi surface, displaying

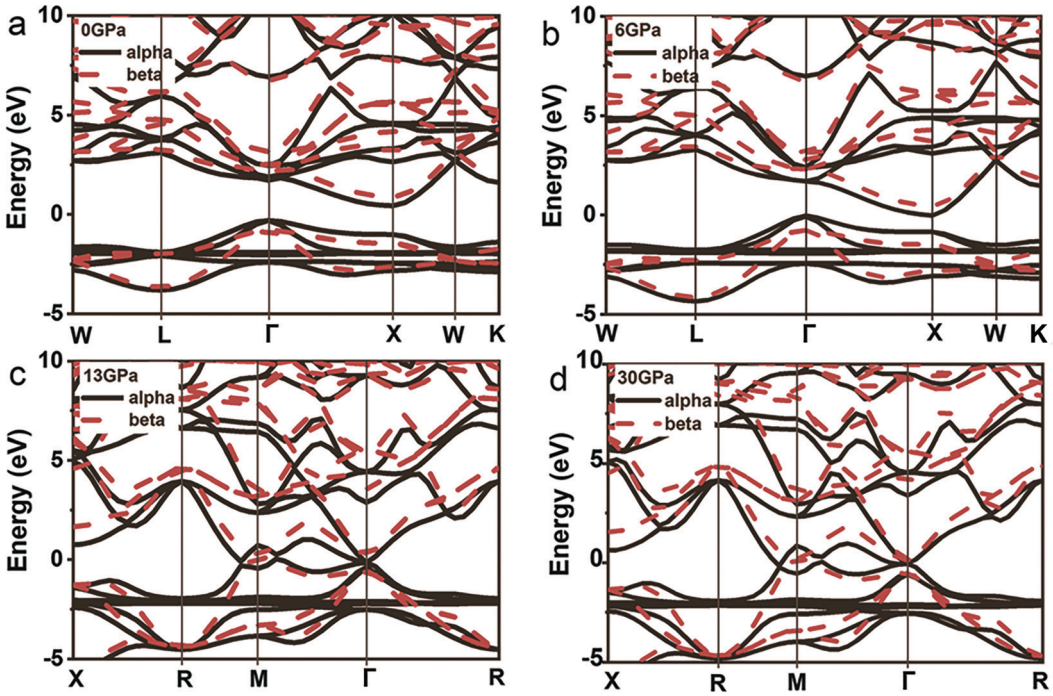

Fig. 3 Energy bands under different pressures. (a) EuTe (NaCl) at 0 GPa; (b) EuTe (NaCl) at 6 GPa; (c) EuTe (CsCl) at 13 GPa; (d) EuTe (CsCl) at 30 GPa.

semimetallic properties. This result can also be observed in Fig. 4a, where the spin-up band gap value has become 0 eV. It is still possible to carry out the analysis of the spin-down band gap change although the total band gap value of the crystal structure becomes 0 eV, providing a basis for further exploration of the high-pressure electronic properties of EuTe. The spin-down band gap value of EuTe does not decrease to zero at 6 GPa, with an energy gap of about 1.237 eV, as shown in Fig. 4b, combined with the 0 eV of spin-up energy band, which proves that EuTe undergoes a semiconductor–semimetal transition at 6 GPa. EuTe still maintains its semimetallic nature under higher pressure because of the spin-down band gap value beyond 0 eV until 12.5 GPa, as can be seen from the energy bands at this pressure (see ESI,† Fig. S1).

It can be concluded that EuTe transforms from semimetal to metal at 13 GPa by calculating the energy band structure of EuTe with CsCl structure, as shown in Fig. 3c. The degree of energy band broadening increases again, and both spin-up and spin-down energy bands are crossed by the Fermi surface. Semimetal–metal transition is due to a pressure-induced structural phase transition, which is based on the pressure point of the phase transition obtained from the principle of enthalpy equivalence. Both the conduction and valence bands of the spin cross the Fermi surface, and increased crossover near the Fermi level is observed in Fig. 3d, which indicates that the no-local nature of the electrons of EuTe gradually increases with increasing pressure, the electron mobility becomes higher, and the metallicity is continuously enhanced.

Density of states describes the distribution of electrons in an energy range. It is necessary to calculate and analyze the total density of states and the fractional wave density of states for both structures, taking the energy at 0 eV as the Fermi surface, in order to better understand the electrical properties of EuTe. The density of states in the energy range of −15 eV to 20 eV was selected for analysis, as the nature of the structure is mainly related to the density of states distributed near the Fermi surface. It can be seen from Fig. 5 that the electronic energy levels of EuTe crystals under atmospheric pressure can be roughly divided into three groups. In the lower valence band from −12.5 eV to −9.5 eV, the density of states is mainly contributed by the s-orbital energy level of Te atoms, which has no obvious interaction with other orbitals and exhibits a strong localization. In the upper valence band from −3 to 0 eV, the contribution is mainly from the f orbitals of Eu atoms and the p orbitals of Te atoms. In the 0–20 eV conduction band region, the contribution is mainly from the s and p orbitals of Te and the d and f orbitals of Eu, and a small amount of the s and p orbitals of Eu original electrons are distributed in this region. The electronic density of states has many similarities with other tellurides.[50] The strong correlation of Eu atoms is worth considering because of its strong f-orbital localization compared to the p-orbital of Te and the d-orbital of Eu. The 4f energy level of Eu atom is formed because the 4f shell layer is located inside the atom and is not perturbed by the external crystal field. In pure elements or compounds, the 4f shell layers do not overlap with each other and form a local energy level. As the pressure increases, the density of states of EuTe decreases slightly, and more peaks appear in the conduction band region (see ESI,† Fig. S2), which are low energy, and the crystal locality is weakened.

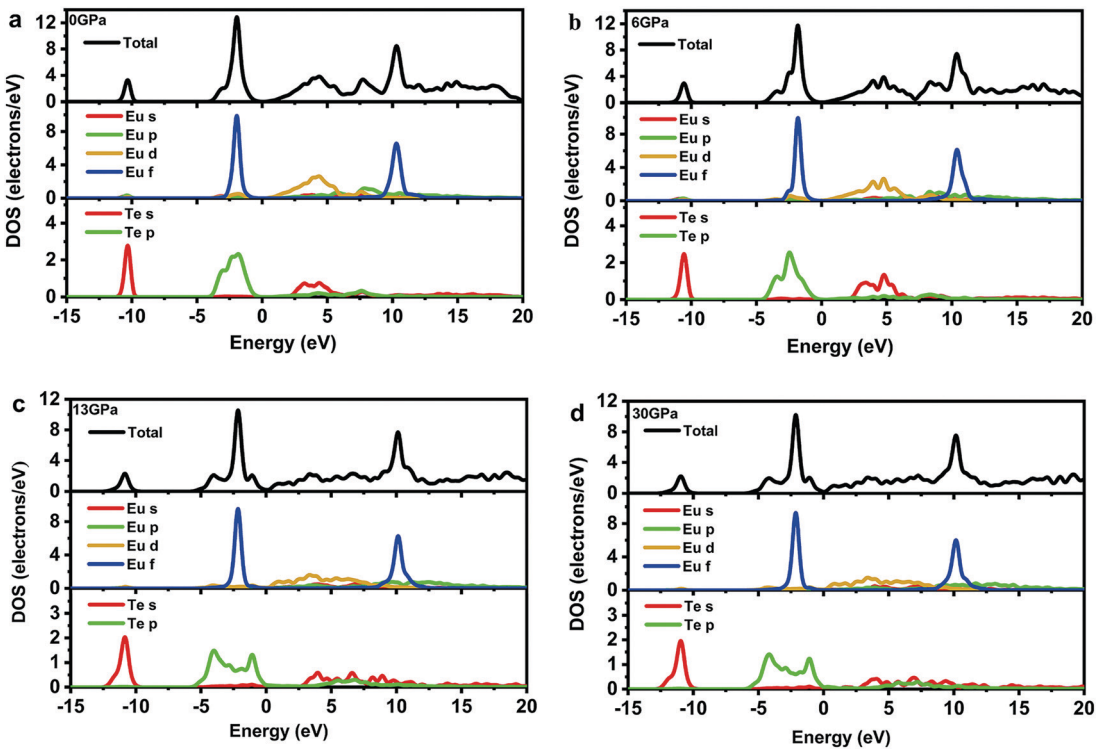

Fig. 5 Density of states under different pressures. (a) EuTe at 0 GPa, (b) EuTe at 6 GPa, (c) EuTe at 13 GPa, (d) EuTe at 30 GPa.

The light absorption and electrical properties of the crystal structure is influenced by the Eu atom because its f-electron orbital is located between the valence band of the anion state and the conduction band of the 6s and 5d states of the rare earth elements.[47] Under pressure, the f–d gap of rare earth atoms starts to close, and the valence state changes due to the transfer or mixing of f and d orbitals at the transition point where the gap closes. While this valence change is not sudden and complete, it is at an intermediate valence between 2^+ and 3^+ at a certain pressure point and gradually increases with increasing pressure until the complete transition to 3^+.[26] The constant shift of the conduction and valence band density of states toward the Fermi surface with increasing pressure is caused by the gradual closure of the gap. Research on the high-pressure behavior of the compounds SmTe, SmS, and SmSe containing the rare earth element Sm found that these three compounds undergo a semiconductor–semimetal transition under the action of external pressure, and this transition is attributed to the transition from Sm^{2+} to Sm^{3+} and delocalization of 4f electrons.[51] Therefore, it can be speculated that this pressure behavior is a general mode of semiconductor rare earth element compounds. In some compounds containing Eu, Ce, Tm and other rare earth ions, there will also be the phenomenon of rare earth ion valence changes leading to metallization phase transitions.

A band gap of about 1.1 eV exists between the f–d orbitals of the NaCl structure at atmospheric pressure (Fig. 5a), indicating that no electron waves exist in the energy interval of −0.6 eV to 0.5 eV, and the chance of electrons existing in the band gap is almost zero when EuTe is a semiconductor. In Fig. 5b, it is observed that EuTe transforms to a semimetallic nature as the pressure increases to 6 GPa, because at this point the f-d orbital is just about to start closing and the Eu atom is between 2^+–3^+. When the structural transition occurs at 13 GPa, the f–d orbital closure increases significantly, and EuTe is metallic in nature, as shown in Fig. 5c, which means that there is no energy interval near the Fermi level where the number of electrons is zero, and the electrons are free electrons that can easily transition from the valence band to the conduction band. At the moment of structural phase transition, the total density of states of EuTe at the Fermi level weakens (see ESI,† Fig. S3), which is mainly caused by the weakening of the density of states of Te atoms. It is not difficult to see from Fig. 5d that EuTe remains metallic in calculations up to 30 GPa because the distribution of density of states does not change significantly compared to 13 GPa, and the s and p electronic states of Eu atoms play a major role in the electrical conductivity. Therefore, it is believed that the distribution of the density of states also indicates that EuTe undergoes a transition from semiconductor to semimetal to metal under pressure.

Fig. 6 shows the additional photoconductivity of EuTe under different pressures, and it can be seen that the highest peaks of additional photoconductivity are basically distributed in the range of 0–2 eV. EuTe has been completely transformed to the semimetallic state when the pressure is increased to 10 GPa, at which time the additional photoconductivity value increases

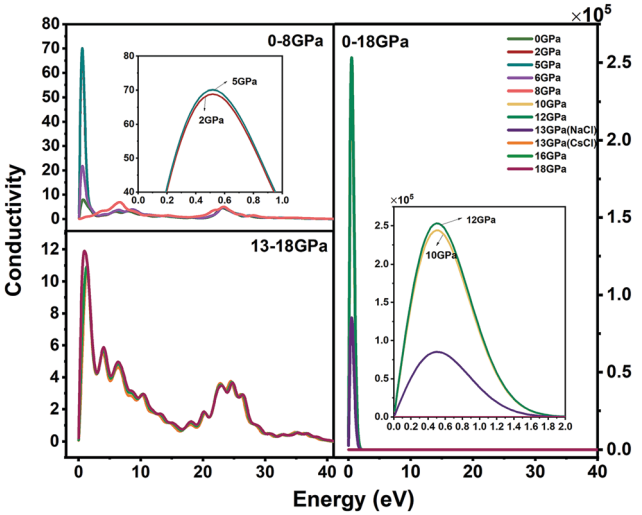

Fig. 6 Variation in the additional photoconductivity of EuTe with energy under different pressures.

significantly compared to the semiconductor state at atmospheric pressure, and photogenerated carriers are generated and moved more easily.

The conversion of EuTe to metal occurs after 13 GPa, at which time the effect of applied pressure on the additional photoconductivity is very weak. Generally, it appears that the additional photoconductivity also varies discontinuously at 6 GPa and 13 GPa. Thus, it is considered that these changes are related to semiconductor–semimetal transition and structural phase transition, respectively.

Pressure-induced resistivity under different temperatures

In order to further verify the theoretical results, high-pressure experiments were also carried out. The temperature-dependent resistivity of the EuTe sample from atmospheric pressure to 35.6 GPa was obtained by high-pressure *in situ* electrical experimental measurements, and the results are shown in Fig. 7. The resistivity trend of semiconductors and metals with temperature is inconsistent, with a negative temperature dependence of the resistivity of semiconductors, while metals are exactly the opposite. It is clear from Fig. 7 that the resistivity of EuTe decreases with increasing temperature, exhibiting semiconductor properties until 13.8 GPa; however, as the pressure increases from 13.8 GPa to 35.6 GPa, the resistivity increases with increasing temperature, exhibiting metallic properties. This experimental result shows that EuTe has undergone a phase transition of electronic structure from semiconductor to metal at approximately 13.8 GPa. The metallization transition of EuTe is closely related to the structural phase transition that occurs at 13 GPa obtained from our theoretical calculations. Rare earth monotelluride compounds are characterized by competition between structural and electronic degrees of freedom, such as in RTe (R = Ce, Pr, Nd, Pm, Sm, Eu, Gd, Tb, Dy, Ho, Er, Tm and Yb), and the degree of their f-electron delocalization determines the sequence of the phase transition.[26] The 4f electron ionization domain allows the transformation of EuTe from a semiconductor

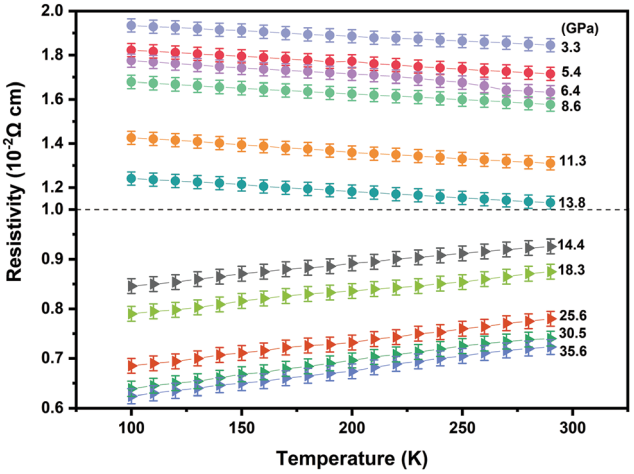

Fig. 7 Temperature-dependent resistivity of EuTe under different pressures.

to a metal, which causes the transformation of NaCl to CsCl structure when the pressure is increased to approximately 13 GPa.

Hall effect and electrical parameters

The variation of carrier parameters *versus* pressure for EuTe was obtained by measurement of the Hall effect. As shown in Fig. 8(a and c), the resistivity (ρ) and Hall coefficient (R_H) both show a downward trend with increasing pressure. Compared with the band gap and the density of states, the resistivity exhibits the change in crystal electronic structure more macroscopically. The change in resistivity under pressure comes mainly from the change in band gap, where the applied pressure affects the number of electrons in the conduction band and the number of holes in the valence band.[52] The resistivity exhibits a trend consistent with our previous theoretical calculation that the band gap value decreases gradually with increasing pressure, implying that EuTe undergoes a semiconductor–semimetal–metal transition, further illustrating the accuracy of our theoretical calculation.

Before 13.8 GPa, $d\rho/dP$ and dR_H/dP are approximately −0.072 and −0.003, respectively; past 13 GPa, they become about −0.001and −0.002. In contrast, the carrier concentration (n) and mobility (μ) both show an upward trend with increasing pressure. The carrier concentration increases with increasing pressure because the band gap of EuTe gradually narrows under pressure, making the energy barrier of carriers lower, and the narrowing of the band gap also leads to a reduction in the effective mass of carriers, which increases the carrier mobility. Before reaching 13 GPa, dn/dP and $d\mu/dP$ are about 0.012 and 1.085 respectively, and after pressurizing to 13.8 GPa, they became approximately 0.011 and 0.237. Discontinuous changes in the slopes of the abovementioned carrier parameters are all caused by the phase transition of NaCl to CsCl structure. It can be seen from the insets of Fig. 8(a and d) that when the pressure is increased to 6.4 GPa, the carrier parameter has a slightly discontinuous change. In the theoretical calculation part, it was concluded that as the pressure increases to 6 GPa, on the one hand, the spin-up energy band broadens across the Fermi surface, and the spin-down energy band has

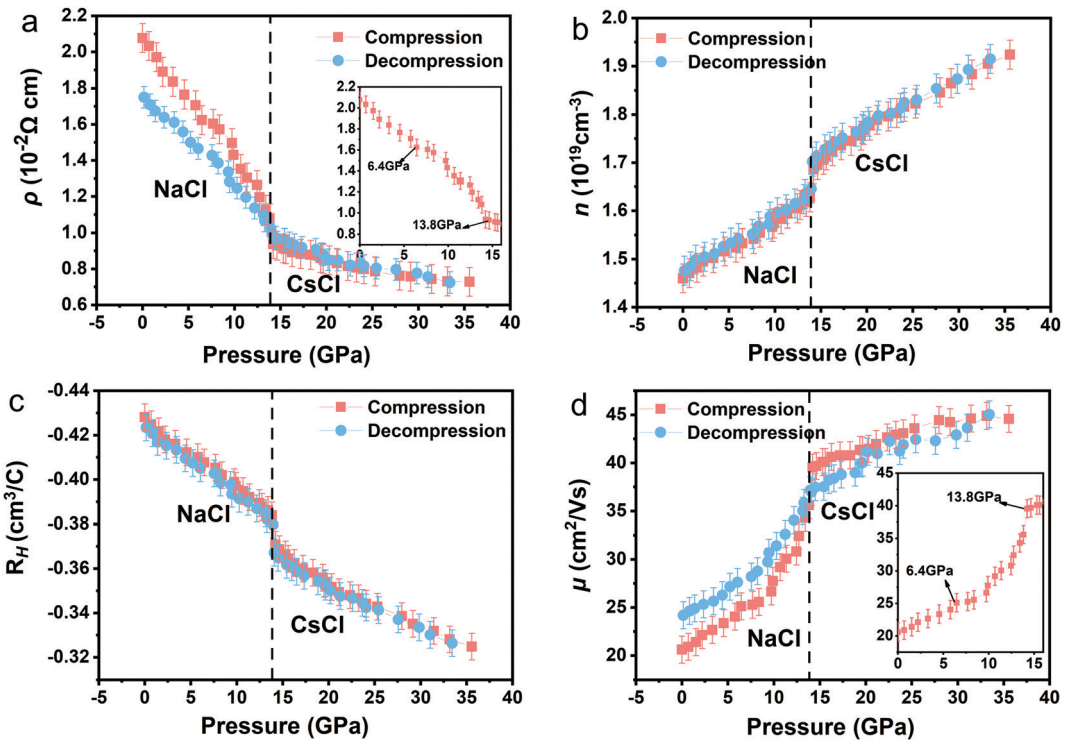

Fig. 8 Electrical parameters under different pressures. Pressure dependence of the (a) resistivity ρ of EuTe, (b) carrier concentration n of EuTe, (c) Hall coefficient R_H of EuTe, (d) mobility μ of EuTe.

an energy gap of 1.237 eV; on the other hand, the f-d orbitals of rare earth elements begin to close, and EuTe is in an intermediate state between 2^+ and 3^+, giving EuTe semimetallic properties. It can be concluded that the changes in spin energy bands and density of states are macroscopically manifested as changes in carrier parameters, yet the discontinuous changes in carrier parameters reflect that EuTe undergoes a semiconductor–semimetal transition. During the decompression, the discontinuous change of carrier parameters at 13.8 GPa is obvious and basically returns to the initial value state, indicating that the structural phase change of EuTe from NaCl to CsCl is reversible. However, there is no obvious change at 6.4 GPa, because the applied pressure shortens the interatomic distance and changes the crystal structure, and when the applied pressure is removed, the interatomic distance cannot return to the initial state in time, leading to a pressure hysteresis phenomenon.

The Hall effect is a very important method to study the physical properties of semiconductors; the basic principle of its generation is that a transverse electric field will be formed in the direction perpendicular to the electric and magnetic fields when a semiconductor with a current is placed in a uniform magnetic field. The resulting Hall electric field on the electrons and the Lorentz force effect cancel each other, and the system reaches a stable state, where the Hall effect satisfies eqn (1):

$$E_y = -\nu_x B_z = -\frac{J_x}{nq} B_z \quad (1)$$

where v_x is the electron drift velocity, B_z is the magnetic field strength, E_y is the Hall electric field perpendicular to the electric field and the magnetic field, and J_x is the current density.

The Hall electric field is proportional to the current density and the magnetic induction intensity:

$$E_y = R_{\mathrm{H}} J_x B_z \quad (2)$$

In eqn (2), R_H is the Hall coefficient, which is obtained by comparing the above eqn (1) and (2):

$$R_{\mathrm{H}} = -\frac{1}{nq} \quad (3)$$

From Fig. 8c, it can be seen that EuTe keeps its n-type structure in the range from atmospheric pressure to 35.6 GPa because the Hall coefficients are always negative. According to eqn (3), the sudden decrease in R_H at 13.8 GPa is due to the sudden increase in n (Fig. 8b).

Pressure-induced photoconductivity properties

The conductivity of a semiconductor depends mainly on the majority carriers when the difference in concentration between the two carriers is significant but the difference in mobility is not. EuTe is an n-type semiconductor with far more electrons than holes, so the contribution of holes to the current is negligible, and the conductivity is expressed as:

$$\sigma = nq\mu_n \quad (4)$$

$$\rho = \frac{1}{\sigma} = \frac{1}{nq\mu_n} \quad (5)$$

The ρ in Fig. 8a suddenly decreased at 13.8 GPa, while n and μ both suddenly increased at 13.8 GPa. It can be seen from the eqn (5) that the discontinuous decrease of ρ at 13.8 GPa is caused by the combination of increasing n and μ (Fig. 8a).

Photoconductivity is defined as the conductivity under green light illumination, because the high-pressure photoconductivity is measured by placing the DAC under green light illumination at a wavelength of 532 nm. Both photoconductivity and conductivity increase with pressure throughout the pressure interval, a phenomenon obtained by observing the photoconductivity and conductivity of EuTe in Fig. 9 under compression and decompression. From Fig. 9(a and b), it can be seen that when pressurized to 6.9 GPa, a slight decrease in photoconductivity and conductivity occurs, which is similar to the carrier parameters, where the change in the conductive properties is affected microscopically by the energy band and density of states, so it can be assumed that this slight discontinuous change is still due to the semiconductor-semimetal transition. With continued increase in pressure, it is evident with the sudden increase in photoconductivity and conductivity at 12.7 GPa and 13.8 GPa, respectively, that their tendencies to change with pressure has changed significantly. According to the results of the theoretical calculations performed above, it is clear that the f and d orbitals of Eu atoms are completely closed when pressurized to about 13 GPa, at which time the electrons move freely between the conduction and valence bands, and EuTe transforms into a metal with a significant increase in electrical conductivity, so the sudden increase in photoelectric conductivity and electrical conductivity can be attributed to the transition from semimetal to metal. The photoconductivity changes discontinuously at approximately 12.7 GPa, which is lower than the pressure point at which the conductivity changes discontinuously at 13.8 GPa, indicating that light has accelerated the transition of EuTe from semiconductor to metal.

The photoconductivity and conductivity in the decompression area both exhibit similar discontinuous phenomena in the vicinity of 12.7 GPa and 13.8 GPa, respectively, and when EuTe is in NaCl structure, the photoconductivity and conductivity are much higher than at a similar pressure zone under compression. When an ideal semiconductor is at absolute zero temperature, the valence band is completely filled with electrons, and the electrons in the valence band cannot be excited to higher energy levels. A reliable method is to use a certain amount of light to irradiate the semiconductor so that the photon energy is equal to or greater than the forbidden bandwidth of the semiconductor to make electrons in the valence band jump across the forbidden band into the empty conduction band to produce electron–hole pairs. In Fig. 9(c and d), the photoconductivity and conductivity are numerically close when EuTe has NaCl structure; however, the photoconductivity has a higher value than the conductivity after EuTe transforms to CsCl structure. This change indicates that the

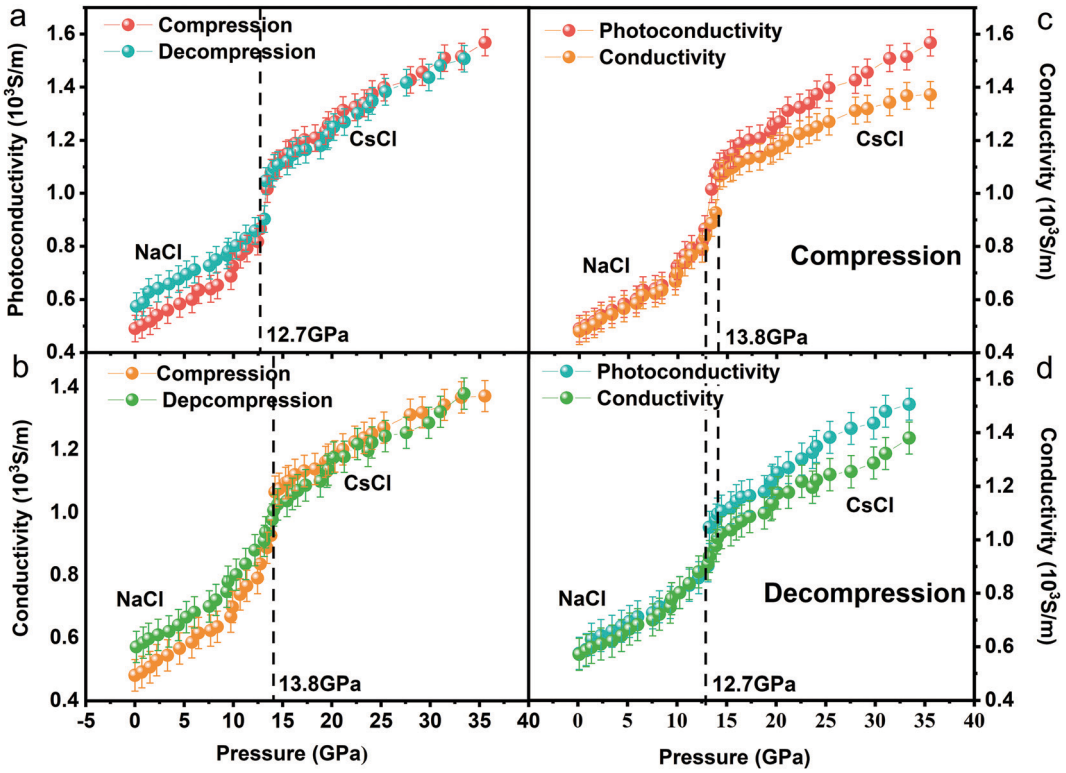

Fig. 9 Pressure dependence of photoconductivity and conductivity. (a) Photoconductivity of EuTe under compression and decompression conditions, (b) conductivity of EuTe under compression and decompression conditions, (c) conductivity and photoconductivity of EuTe under compression, (d) conductivity and photoconductivity of EuTe under decompression.

electrons can be excited to the conduction band under higher pressure due to reduction of the band gap value to a value less than or equal to the photon energy, which makes the photoconductivity increase, so the pressure may have a facilitating effect on the excitation of electrons.

Conclusions

In summary, the broadening energy band reflects the fact that EuTe undergoes a semiconductor–semimetal–metal transition, and the degree of closure of the density of states likewise supports this conclusion. The trends in photoconductivity for EuTe under different pressures are consistent with the discontinuous changes at 6.9 GPa and 13.8 GPa, which are caused by the semiconductor–semimetal transition and structural phase transition, respectively. The temperature-dependent resistivity demonstrates that EuTe undergoes a metallization transition at 13.8 GPa. The discontinuous electrical parameters reflect the structural phase transition of EuTe from the NaCl structure to CsCl structure. At approximately 13.8 GPa, the abrupt decrease in resistivity is caused by the combined increase in carrier concentration and mobility, while the abrupt decrease in the Hall coefficient is due to the increase in carrier concentration. The pressure point at which the metallization transition of EuTe occurs is advanced to about 12.7 GPa due to the effect of light, and pressure may have a facilitating effect on the excitation of electrons to a certain extent.

Author contributions

Y. L. and P. N. contributed to conceptualisation and resources, as well as provided supervision and administered the project. Y. L., J. L., P. Z., X. L., and J. Z. performed software simulations. Y. L., Q. J., N. X. and P. Z. acquired funding for the project. Y. L., J. L., J. Z., L. Y., Q. J., and P. N. carried out the formal analysis of the data and wrote the manuscript.

Conflicts of interest

There are no conflicts to declare.

Acknowledgements

This work was supported by the National Natural Science Foundation of China (Grant No. 11804336, 11804249, 11804194); the Natural Science Foundation of Tianjin City (Grant No. 18JCQNJC03700); and the Science & Technology Development Fund of Tianjin Education Commission for Higher Education (Grant No. 2018KJ210, 2017ZD06).

References

1 S. Belhachi, *Spin*, 2018, **8**, 4.

2 B. Diaz, E. Granado, E. Abramof, P. H. O. V. Rappl, A. Chitta and A. B. Henriques, *Phys. Rev. B: Condens. Matter Mater. Phys.*, 2008, **78**, 13.
3 A. B. Henriques and P. A. Usachev, *Phys. Rev. B*, 2017, **96**, 19.
4 V. V. Pavlov, R. V. Pisarev, S. G. Nefedov, I. A. Akimov, D. R. Yakovlev, M. Bayer, A. B. Henriques, P. H. O. Rappl and E. Abramof, *J. Appl. Phys.*, 2018, **123**, 19.
5 L. Kilanski, M. Gorska, M. Arciszewska, A. Podgorni, R. Minikayev, B. Brodowska, A. Reszka, B. J. Kowalski, V. E. Slynko and E. I. Slynko, *Acta Phys. Pol., A*, 2018, **134**, 950–953.
6 M. Lafrentz, D. Brunne, B. Kaminski, V. V. Pavlov, A. B. Henriques, R. V. Pisarev, D. R. Yakovlev, G. Springholz, G. Bauer, E. Abramof, P. H. O. Rappl and M. Bayer, *Phys. Rev. B: Condens. Matter Mater. Phys.*, 2010, **82**, 23.
7 E. Heredia, B. Diaz, A. Malachias, P. H. O. Rappl, F. Iikawa, M. J. S. P. Brasil and P. Motisuke, *J. Cryst. Growth*, 2014, **386**, 139–145.
8 E. Heredia, P. Motisuke, P. H. de Oliveira Rappl, M. J. S. P. Brasil and F. Iikawa, *Appl. Phys. Lett.*, 2012, **101**, 9.
9 A. B. Henriques, A. R. Naupa, P. A. Usachev, V. V. Pavlov, P. H. O. Rappl and E. Abramof, *Phys. Rev. B*, 2017, **95**, 4.
10 A. B. Henriques, G. D. Galgano, P. H. Rappl and E. Abramof, *Phys. Rev. B*, 2016, **93**, 20.
11 B. Kaminski, M. Lafrentz, R. V. Pisarev, D. R. Yakovlev, V. V. Pavlov, V. A. Lukoshkin, A. B. Henriques, G. Springholz, G. Bauer, E. Abramof, P. H. O. Rappl and M. Bayer, *Phys. Rev. B: Condens. Matter Mater. Phys.*, 2010, **81**, 15.
12 L. Wang, B. Li, X. Zhao, C. Chen and J. Cao, *PLoS One*, 2012, **7**, 6.
13 S. Ghosh and H. Ghosh, *J. Phys. Chem. Solids*, 2021, **133**, 109993.
14 K. Guo, Z. Man, Q. Cao, H. Chen, X. Guo and J. Zhao, *Chem. Phys.*, 2011, **380**, 54–60.
15 T. Ohnishi, T. Taniguchi, A. Ikoshi, S. Mizusaki, Y. Nagata, S. Lai, M. Lan, Y. Noro, T. C. Ozawa, K. Kindo, A. Matsuo and S. Takayanagi, *J. Alloys Compd.*, 2010, **506**, 27–32.
16 J. Zhang, N. Zhao, W. Wei and Y. Sun, *Int. J. Hydrogen Energy*, 2010, **35**, 11776–11786.
17 D. Tchon, D. Bowskill, I. Sugden, P. Piotrowski and A. Makal, *J. Mater. Chem. C*, 2021, **9**, 2491–2503.
18 L. Yang, J. Jiang, L. Dai, H. Hu, M. Hong, X. Zhang, H. Li and P. Liu, *J. Mater. Chem. C*, 2021, **9**, 3692.
19 J. Shi, W. Cui, J. Hao, M. Xu, X. Wang and Y. Li, *Nat. Commun.*, 2020, **11**, 1.
20 Y. Akahama, S. Kawaguchi, N. Hirao and Y. Ohishi, *Appl. Phys. Lett.*, 2020, **117**, 18.
21 I. S. Lyubutin, I. S. Lyubutin, S. S. Starchikov, A. G. Gavriliuk, I. A. Troyan, Yu. A. Nikiforova, A. G. Ivanova, A. I. Chumakov and R. Ruffer, *Appl. Phys. Lett.*, 2018, **112**, 24.
22 R. F. Service, *Science*, 2020, **370**, 273–274.
23 C. R. Johnson, G. M. Tsoi and Y. K. Vohra, *J. Phys.: Condens. Matter*, 2017, **29**, 6.
24 R. K. Arslanov, T. R. Arslanov, I. V. Fedorchenko and A. Zheludkevich, *J. Exp. Theor. Phys.*, 2020, **130**, 94–100.
25 D. Singh, V. Srivastava, M. Rajagopalan, M. Husain and A. K. Bandyopadhyay, *Phys. Rev. B: Condens. Matter Mater. Phys.*, 2001, **64**, 11.
26 L. Petit, A. Svane, M. Lueders, Z. Szotek, G. Vaitheeswaran, V. Kanchana and W. M. Temmerman, *J. Phys.: Condens. Matter*, 2014, **26**, 27.
27 I. N. Goncharenko and I. Mirebeau, *Europhys. Lett.*, 1997, **37**, 9.
28 A. Chatterjee, A. K. Singh and A. Jayaraman, *Phys. Rev. B: Condens. Matter Mater. Phys.*, 1972, **6**, 2285–2291.
29 M. Ishizuka, Y. Kai, R. Akimoto, M. Kobayashi, K. Amaya and S. Endo, *Magn. Magn. Mater.*, 1997, **166**, 211–215.
30 N. F. Oliveira, S. Foner, Y. Shapira and T. B. Reed, *Phys. Rev. B: Condens. Matter Mater. Phys.*, 1972, **5**, 2634–2646.
31 Y. Shapira, S. Foner, N. F. Oliveira and T. B. Reed, *Phys. Rev. B: Condens. Matter Mater. Phys.*, 1972, **5**, 2647–2657.
32 Y. Shapira, S. Foner and N. F. Oliveira, *Phys. Lett. A*, 1970, **33**, 5.
33 A. B. Henriques, F. C. D. Moraes, G. D. Galgano, A. J. Meaney, P. C. M. Christianen, J. C. Maan, E. Abramof and P. H. O. Rappl, *Phys. Rev. B: Condens. Matter Mater. Phys.*, 2014, **90**, 16.
34 A. B. Henriques, M. A. Manfrini, P. H. O. Rappl and E. Abramof, *Phys. Rev. B: Condens. Matter Mater. Phys.*, 2008, **77**, 3.
35 A. Gour, S. Singh and R. K. Singh, *J. Phys. Chem. Solids*, 2007, **69**, 1669–1675.
36 M. D. Segall, P. J. D. Lindan, M. J. Probert, C. J. Pickard, P. J. Hasnip and M. C. Payne, *J. Phys.: Condens. Matter*, 2001, **14**, 2717–2744.
37 T. H. Fischer and J. Almlof, *J. Phys. Chem.*, 1992, **96**, 9768–9774.
38 Y. Han, C. Gao, Y. Ma, H. Liu, Y. Pan, J. Luo, M. Li, C. He, X. Huang and G. Zou, *Appl. Phys. Lett.*, 2005, **86**, 6.
39 Y. Li, J. Liu, P. Zhang, J. Zhang, N. Xiao, L. Yu and P. Niu, *J. Mater. Sci.*, 2020, **55**, 14873–14882.
40 D. Errandonea, A. Munoz and J. Gonzalez-Platas, *J. Appl. Phys.*, 2014, **115**, 043507.
41 Y. Li, Y. Gao, Y. Han, C. Liu, W. Ren, Q. Wang, Y. Ma, B. Wu and C. Gao, *J. Phys. Chem. C*, 2012, **116**, 25198–25205.
42 G. J. Piermarini, S. Block, J. D. Barnett and R. A. Forman, *J. Appl. Phys.*, 1975, **46**, 2774–2780.
43 H. Mao, J. Xu and P. M. Bell, *J. Geophys. Res.*, 1986, **91**, 4673–4676.
44 D. Errandonea, A. Segura, D. Martinez-Garcia and V. Munoz-San Jose, *Phys. Rev. B: Condens. Matter Mater. Phys.*, 2009, **79**, 309–314.
45 Y. Ma, A. R. Oganov, Z. Li, Y. Xie and J. Kotakoski, *Phys. Rev. Lett.*, 2009, **102**, 6.
46 Y. Ma, M. Eremets, A. R. Oganov, Y. Xie, I. Trojan, S. Medvedev, A. O. Lyakhov, M. Valle and V. Prakapenka, *Nature*, 2009, **458**, 182–185.

47 A. Jayaraman and A. K. Singh, *Phys. Rev. B: Condens. Matter Mater. Phys.*, 1974, **9**, 2513–2520.
48 D. C. Gupta and K. C. Singh, *J. Mol. Model.*, 2011, **18**, 3003–3012.
49 D. Diaz-Anichtchenko, L. Gracia and D. Errandonea, *RSC Adv.*, 2021, **11**, 10401–10415.
50 V. Bilovol, M. Fontana, J. A. Rocca, H. H. Medina Chanduvi, A. M. Mudarra Navarro, A. V. Gil Rebaza, L. A. Errico, A. Liang, D. Errandonea and A. M. Urena, *J. Alloys Compd.*, 2020, **845**, 156307.
51 A. Jayaraman, V. Narayanamurti, E. Bucher and R. G. Maines, *Phys. Rev. Lett.*, 1970, **25**, 1430–1433.
52 C. Yu, Q. Yu, C. Gao, H. Yang, B. Liu, G. Peng, Y. Han, D. Zhang, X. Cui, C. Liu, Y. Wang, B. Wu, C. He, X. Huang and G. Zou, *J. Appl. Phys.*, 2008, **103**, 11.